Int. Conf. on Jets, Wakes and Separated Flows, ICJWSF-2017
October 9-12, 2017, Cincinnati, Ohio USA

BI-STABLE STATES IN THE WAKE OF A 35° AHMED BODY AT YAW

*[1]A. Rao, [1]G. Minelli, [2]B. Basara and [1]S. Krajnović

[1]Vehicle Aerodynamics Laboratory (*VAL*), Department of Mechanics and Maritime Sciences, Chalmers University of Technology, Gothenburg 41296, Sweden.

[2]AVL List GmbH, Advanced Simulation Technologies, Hans-List-Platz 1, 8020 Graz, Austria.

anirudh.rao@chalmers.se

ABSTRACT

Recent experimental observations by in the wake of a 35° back slant Ahmed body reveal the existence of two stable states when the body is yawed [1]. The two flow states, flow state I and flow state II, are confirmed numerically by using the partially-averaged Navier–Stokes (PANS) formulation on unstructured meshes. Flow state I corresponds to a low drag/low lift state with the flow being fully separated, while flow state II corresponds to a high drag/high lift state, with the flow separating and reattaching over the back slant. For the Ahmed body at zero yaw angle ($\beta = 0°$), flow state I is observed. This flow state is observed as the yaw angle is increased up to $|\beta| \simeq 12.5°$. As the yaw angle is increased beyond $|\beta| = 12.5°$, flow state II is observed. These findings are in good comparison with the experimental observations of [1].

1 INTRODUCTION

The *Ahmed body* [2] is an idealised car model and is representative of an automobile hatchback. It consists of a rounded front edge, a flat roof and bottom, a slanted rear window and a vertical base. The angle of slanted section is critical to the flow structures that are observed downstream of the body. The flow consists of a pair of longitudinal vortices (also known as the C-pillar vortices) on either side of the body, a region of separated (or attached) flow behind the back slant and a pair of recirculation zones behind the vertical base. The conceptual model of the flow structures in the wake are presented in figure 6 of [2], and [3]. For back slant angles less than 30°, the flow which separates at the intersection of the roof edge - back slant interface, reattaches further downstream on the back slant. For larger back slant angles, the flow does not reattach and is fully separated over the back slant. [2] observed that the drag coefficient increased up to the critical angle of 30° as the back slant angle was increased, beyond which a low drag state was observed. In this study, we refer to the former as flow state II, and to the latter as flow state I. The two flow states have also been observed in both experimental and numerical works ([4], [5], [6], [7], [8], [9] and others). The occurrence of the two flow states can be manipulated by actively changing the back slant angle by the use of an deflector [10].

The influence of the width of the 25° back slant Ahmed body on the occurrence of the two flow states was investigated by [9]. As the aspect ratio (defined as the width of the model under consideration to the standard width Ahmed body) was increased beyond $\simeq 0.85$, the flow state changed from state II to state I. A sharp decrease in the lift and drag coefficients was observed as the transition occurred. In a similar water channel investigation, [8] observed this discontinuity to occur for aspect ratios $\simeq 1 - 1.1$. This indicates that the standard width Ahmed body is at a critical juncture between the two flow states. More recently, [11] observed that the occurrence of the two flow states depends not only on the back slant angle, but also on the aspect ratio (defined as the ratio of the width of the Ahmed body considered to the width of the standard Ahmed body). They showed that flow state II is observed for short aspect ratio bodies, even at large values of the back slant angle. They hypothesised that at values closes to criticality, the separated flow behind the back slant merged with the recirculating zones behind the vertical back face, leading to fully separated flow behind the body.

The influence of the yaw angle on the two flow states was explored by [1] for $|\beta| \leqslant 25°$ for the 25° and 35° back slant angle Ahmed bodies (also see

[12]). For the 25° Ahmed body, flow state II was observed for the entire range of yaw angles, with the drag force coefficient showing a monotonous increase with increase in the yaw angle. For the 35° back slant angle, flow state I which was observed at 0° (in line flow), was observed up to $\beta \lesssim 10°$. For $10° \lesssim |\beta| \lesssim 14°$, the flow was found to alternate between flow states I and II, and for $\beta \gtrsim 15°$, flow state II was observed, The switching between the two states was most pronounced at $|\beta| = 12.5°$. [1] speculated that the switching behaviour was random, with minor upstream disturbances causing the flow to switch from one state to the other. A similar observation was reported by [13] for a commercial hatchback vehicle.

The current study aims to replicate the results of [1] using the partially-averaged Navier–Stokes (PANS) turbulence model on unstructured meshes. The remainder of the article is organised as follows: section 2 briefly details the problem setup and numerical formulation, followed by results in section 3, and conclusions in section 4.

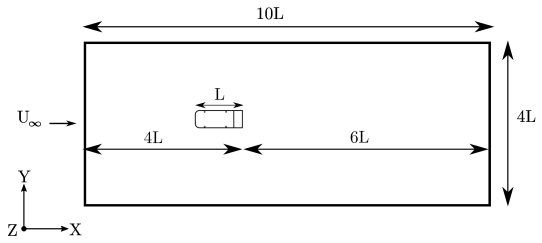

Figure 1: Schematic of the problem under consideration.

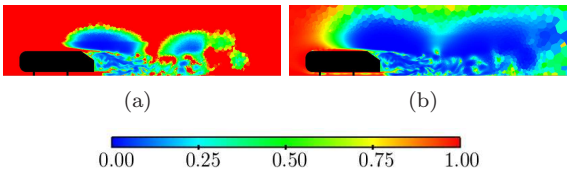

Figure 2: Comparison of the contours of (a) input f_k, and (b) output f_k for the Ahmed body at zero yaw angle at $U_\infty = 30\text{ms}^{-1}$ in the $Y = 0$ plane. Flow is from left to right in these images.

2 METHODOLOGY

2.1 PROBLEM SETUP

The Ahmed body, as described in [2], with a back slant angle of 35° is used for the numerical investigation. The Reynolds number based on the length ($L = 1.044$m) and the incoming flow velocity of $U_\infty = 30\text{ms}^{-1}$ corresponds to a value of $Re \simeq 2 \times 10^6$. Figure 1 shows the schematic of the problem under consideration. The computational domain is $10L$ in length with the Ahmed body placed $4L$ downstream from the inlet. The width and height of the domain are $4L$ and $2L$, respectively. For cases where the influence of the yaw angle is investigated, the Ahmed body is rotated about a point midway between the cylindrical supports. Polyhedral elements are used to construct the mesh using AVL FAME$^{\text{TM}}$ M software. Twelve prism layers were used to capture the boundary layer and three refinement regions of increasing polyhedral sized elements were used around the body. The resulting cell count was approximately 10 - 18 million, depending on the yaw angle. The sides and the top surfaces of the domain are assigned symmetry boundary conditions, while the Ahmed body and the ground surfaces are assigned no-slip wall condition.

2.2 NUMERICAL FORMULATION

PANS is a bridging turbulence closure model between the Reynolds averaged Navier–Stokes (RANS) and direct numerical simulations (DNS) ([14], [15]), and its implementation in AVL FIRE$^{\text{TM}}$ has been used to investigate a wide range of bluff body flows ([16], [17], [18], [19]). The PANS formulation is a non-zonal method, whereby it adapts to the computational grid, resolving the flow structures in regions where the grid resolution is adequate and using RANS turbulence modelling where the resolution is sparse. The control parameters used to ensure a smooth switch are f_k and f_e, which are the ratios of the unresolved to the total kinetic energy and unresolved to the total dissipation, respectively. f_k which is computed by $f_k = \frac{1}{\sqrt{C_\mu}}\left(\frac{\Delta}{\Lambda}\right)^{2/3}$, where $C_\mu = 0.22$, $\Lambda = \frac{(k_{unresolved}+k_{resolved})^{3/2}}{\varepsilon}$,$\Delta = (\Delta_x\Delta_y\Delta_z)^{1/3}$; and $f_e = 1$ is assumed. The PANS asymptotic behaviour goes smoothly from RANS to DNS as f_k decreases from one to zero. Accordingly, f_k is implemented as a dynamic parameter, changing at each grid node and is evaluated at each time-step. For more details on the numerical formulation and the PANS equations, the reader is referred to [20, 21, 22] and the references therein. Shown in figures 2(a) and 2(b) are the contours of the input f_k computed by the above formula, and the output f_k computed by the ratio of the unresolved to the total turbulent kinetic energy, respectively. Clearly, lower values of f_k are observed in the wake, indicating that the flow structures are adequately resolved. Furthermore, the input f_k computed by the formula at is still a conservative estimate.

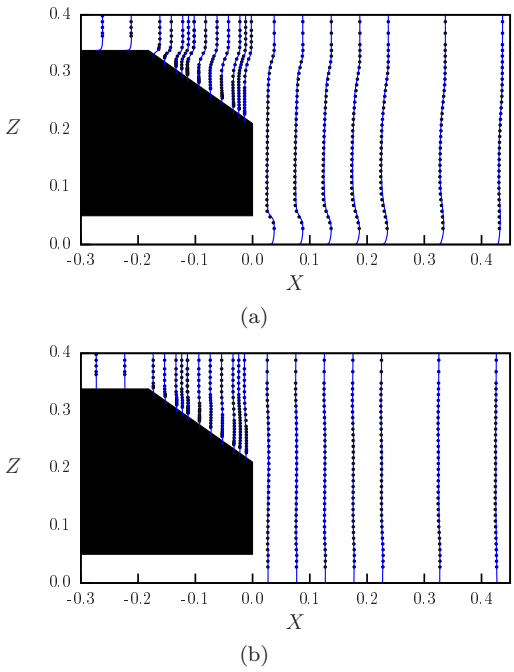

Figure 3: Comparison of the time-averaged velocity profiles for the 35° back slant Ahmed body at $U_\infty = 30\text{ms}^{-1}$ (blue lines) with the experimental data (•) from [26] in the $Y = 0$m plane. (a) Streamwise velocity profiles, and (b) vertical velocity profiles are compared for streamwise locations along the back slant and the near wake.

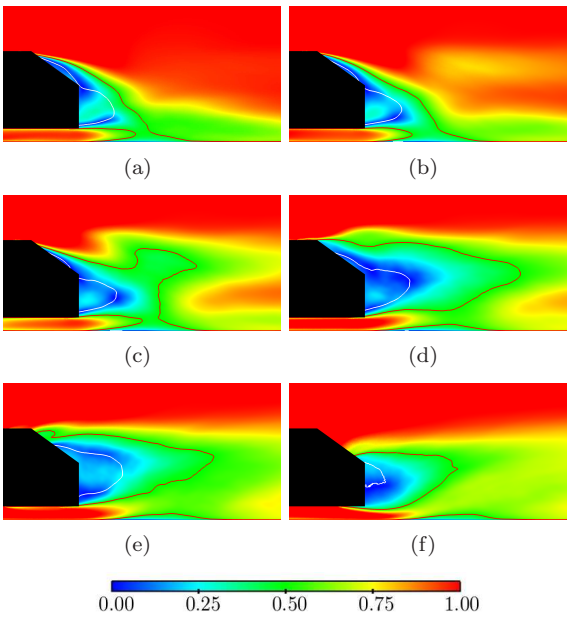

Figure 4: Visualisation of the velocity contours ($\sqrt{u^2+w^2}/U_\infty$) for the 35° back slant Ahmed body in flow state I at $\beta = -12.5°$ at the specified planes: (a) $Y = 0.12$m, (b) $Y = 0.16$m, (c) $Y = 0.20$m, (d) $Y = 0.24$m, (e) $Y = 0.28$m and (f) $Y = 0.32$m. Isotachs of $\sqrt{u^2+w^2}/U_\infty = 0.5$ and $u/U_\infty = 0$ are indicated by the red and white lines, respectively. u and w are the streamwise and the vertical flow components of the velocity, respectively. Flow is from left to right in these images.

The PANS equations are discretised using the commercial finite volume solver to solve the incompressible Navier–Stokes equations using a collocated grid arrangement [23]. The code has previously been used to investigate the flow past bodies at yaw over a wide range of Reynolds numbers ([24], [25], [21]).

3 RESULTS

The flow past the 35° back slant Ahmed body at zero yaw angle is first validated with the experimental data of [26] obtained from the ERCOFTAC database [27]. Shown in figures 3(a) and 3(b) are the comparison of the time-averaged streamwise and vertical velocity profiles obtained from the PANS simulation with the LDA data. These profiles are in good comparison with their experimental counterparts. Flow state I is observed behind the Ahmed body, with separation behind the back slant.

Next, the Ahmed body is yawed about a point midway between the cylindrical supports. As the yaw angle is increased, asymmetrical flow is observed, with vortices emanating from the front of the body. On the windward side, the roof-top vortex from the front of the body merges with the C-pillar vortex as they rotate in the same direction, while on the leeward side, the two vortices do not combine. Simulations performed at $\beta = -10°$ and $\beta = \pm 12.5°$ show flow state I being observed. Shown in figure 4 are the contours of the normalised time-averaged velocity fields at the specified planes for $\beta = -12.5°$. These images can be compared with figure 14 of [1].

Shown in figure 5 are the contours of the normalised time-averaged velocity fields at the specified planes for $\beta = -15°$. The flow remains in state II for this case, with high values of lift and drag being observed. These images can be compared with figure 15 of [1], although in their case, the high drag state (state II) for $\beta = -12.5°$ is shown. The numerical simulations predict a larger downwash for as compared to the experimental visualisations. Nonetheless, these images compare reasonably well with their experimental counterparts.

Shown in figures 6(a) and 6(b) are the contours of the pressure coefficient for flow state I at $\beta = -12.5°$ and flow state II at $\beta = -15°$, respectively. In flow state I, higher pressure coefficient is observed over the back slant, leading to a low

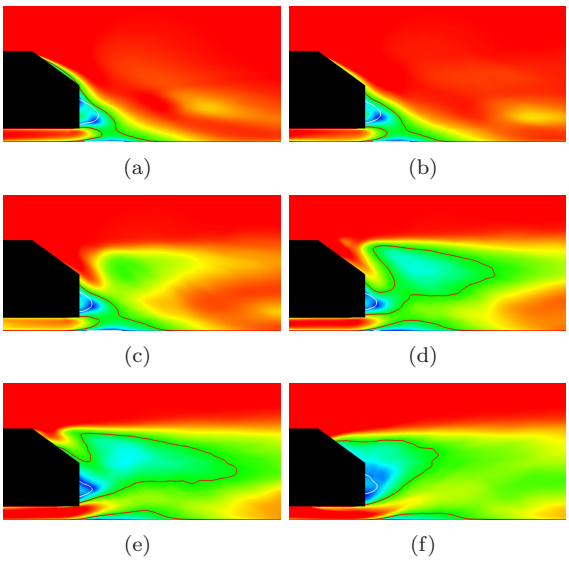

Figure 5: Visualisation of the velocity contours ($\sqrt{u^2+w^2}/U_\infty$) for the 35° back slant Ahmed body in flow state II at $\beta = -15°$ at the specified planes: (a) $Y =$ 0.12m, (b) $Y = 0.16$m, (c) $Y = 0.20$m, (d) $Y = 0.24$m, (e) $Y = 0.28$m and (f) $Y = 0.32$m. Flow is from left to right in these images. Contour shading is as per figure 4.

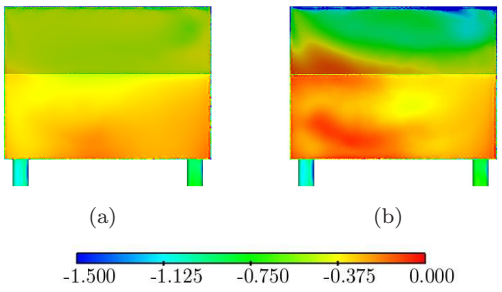

Figure 6: Contour plots of the pressure coefficient for the 35° back slant angle Ahmed body viewed from behind the body for (a) state I - $\beta = -12.5°$, and (b) state II - $\beta = -15°$.

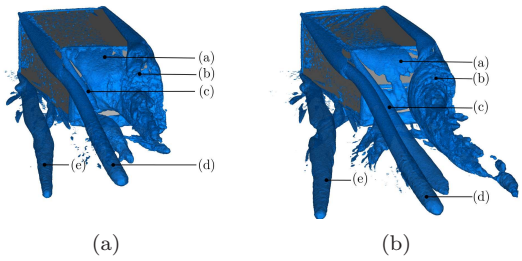

Figure 7: Isosurfaces of the λ_2 ($\lambda_2 = -5000s^{-2}$) for (a) state I - $\beta = -12.5°$, and, (b) state II - $\beta = -15°$. In each subfigure, the flow over the back slant (a), the merged windward side roof-edge vortex and C-pillar vortex (b), the C-pillar vortex on the leeward side (c), the roof-edge vortex on the leeward side, and the bottom-edge vortex (e) are marked. Flow is from top to bottom in these images.

drag state for this case. In flow state II, the windward side C-pillar vortex aids the flow to reattach over the back slant, leading to more downwash over the back slant as compared to flow state I. A lower pressure region is observed over the back slant and the vertical back face for $\beta = -15°$, which leads to a higher drag coefficient, despite the higher pressure observed on the leeward side of the Ahmed body (left side of the image in figure 6(b)) as compared to the windward side. Clearly discernible is the imprint of the C-pillar vortex in flow state II, indicating that it is closer to the back slant as compared to flow state I.

Lastly, to obtain a qualitative representation of flow state I and II, isosurfaces of λ_2 (see [28]) based on the time-averaged velocities are shown in figures 7(a) and 7(b), respectively. The various flow structures in the two flow states are identified. In flow state I ($\beta = -12.5°$), the separation behind the back slant is observed with a weak windward side vortex. The C-pillar vortex on the leeward side is shorter as compared to flow state II ($\beta = -15°$). The stronger windward side vortex and the C-pillar vortex on the leeward side, aid the reattachment of the flow on the back slant in flow state II. Furthermore, a larger amount of the flow from the windward side of the Ahmed body is drawn in to the windward side vortex, resulting in a larger and stronger vortex structure. Also seen in these images are the vortical structures from the cylindrical supports.

4 CONCLUSIONS

The two flow states which have previously been observed in the wake of 35° back slant angle Ahmed body at yaw is investigated using the PANS turbulence model on unstructured meshes, For $|\beta| \leqslant 12.5°$, flow state I was observed and for $\beta = -15°$, flow state II was observed. These findings are consistent with the observations of [1]. It may be noted that the switching behaviour reported in their experimental work was not observed here, due to the rather short run times used. [1] noted that the switch in the two flow states could be triggered by random upstream disturbances. These disturbances could trigger changes in the flow downstream, leading to the merging of the recirculation regions behind the vertical base and back slant, leading to flow state I [11, 29]. Thus, a number of factors such as the back slant angle, aspect ratio and yaw angle in-

fluence the wake behind an Ahmed body, leading to the two wake states.

5 ACKNOWLEDGEMENTS

The authors would like to thank the computational support provided by Chalmers Centre for Computational Science and Engineering (C3SE) and National Supercomputer Centre (NSC), Linköping University provided by the Swedish National Infrastructure for Computing (SNIC). The authors would also like to acknowledge the support and licences provided by AVL GmbH, Austria.

REFERENCES

[1] W. Meile, T. Ladinek, G. Brenn, A. Reppenhagen, and A. Fuchs. Non-symmetric bistable flow around the Ahmed body. *International Journal of Heat and Fluid Flow*, 57:34 – 47, 2016.

[2] S. R. Ahmed, G. Ramm, and G. Faltin. Some salient features of the time-averaged ground vehicle wake. In *SAE Technical Paper, 840300*. SAE International, 1984.

[3] B. F. Zhang, Y. Zhou, and S. To. Unsteady flow structures around a high-drag Ahmed body. *Journal of Fluid Mechanics*, 777:291–326, 2015.

[4] E. Guilmineau, G.B. Deng, A. Leroyer, P. Queutey, M. Visonneau, and J. Wackers. Assessment of hybrid RANS-LES formulations for flow simulation around the Ahmed body. *Computers and Fluids*, page available online, 2017.

[5] B. Conan, J. Anthoine, and P. Planquart. Experimental aerodynamic study of a car-type bluff body. *Experiments in Fluids*, 50(5):1273–1284, 2011.

[6] E. Guilmineau, Deng G. B., and J. Wackers. Numerical simulation with a DES approach for automotive flows. *Journal of Fluids and Structures*, 27(5–6):807 – 816, 2011.

[7] H. Lienhart, C. Stoots, and S. Becker. Flow and turbulence structures in the wake of a simplified car model (Ahmed model). In *New Results in Numerical and Experimental Fluid Mechanics III: Contributions to the 12th STAB/DGLR Symposium Stuttgart, Germany 2000*, pages 323–330, Berlin, Heidelberg, 2002.

[8] J. Venning, D. Lo Jacono, D. Burton, M. Thompson, and J. Sheridan. The effect of aspect ratio on the wake of the Ahmed body. *Experiments in Fluids*, 56(6):126, 2015.

[9] M. Corallo, J. Sheridan, and M. C. Thompson. Effect of aspect ratio on the near-wake flow structure of an Ahmed body. *Journal of Wind Engineering and Industrial Aerodynamics*, 147:95 – 103, 2015.

[10] D. Kim, H. Lee, W. Yi, and H. Choi. A bio-inspired device for drag reduction on a three-dimensional model vehicle. *Bioinspiration and Biomimetics*, 11(2):026004, 2016.

[11] I. Kohri, Y. Kobayashi, A. Kasai, T. Nasu, D. Katoh, and Y. Hashizume. Experimental analysis on the transitional mechanism of the wake structure of the Ahmed body. *SAE Int. J. Passeng. Cars - Mech. Syst.*, 9:612–624, 04 2016.

[12] F. J. Bello-Millán, T. Mäkelä, L. Parras, C. del Pino, and C. Ferrera. Experimental study on Ahmed's body drag coefficient for different yaw angles. *Journal of Wind Engineering and Industrial Aerodynamics*, 157:140 – 144, 2016.

[13] G. Bonnavion, O. Cadot, A. Évrard, V. Herbert, S. Parpais, R. Vigneron, and J. Délery. On multistabilities of real car's wake. *Journal of Wind Engineering and Industrial Aerodynamics*, 164:22 – 33, 2017.

[14] S. S. Girimaji, R. Srinivasan, and E. Jeong. PANS turbulence model for seamless transition between RANS and LES: Fixed-point analysis and preliminary results. *Journal of Applied Mechanics, Transactions ASME*, 2(3):1901–1909, 2003.

[15] S. S. Girimaji. Partially-Averaged Navier-Stokes model for turbulence: A Reynolds-Averaged Navier-Stokes to direct numerical simulation bridging method. *Journal of Applied Mechanics, Transactions ASME*, 73(3):413–421, 2006.

[16] S. Jakirlic, L. Kutej, D. Hanssmann, B. Basara, T. Schütz, and C. Tropea. Rear-end shape influence on the aerodynamic properties of a realistic car model: A RANS and Hybrid LES/RANS study. In *New Results in Numerical and Experimental Fluid Mechanics X: Contributions to the*

19th STAB/DGLR Symposium Munich, Germany, 2014, pages 397–407. Springer International Publishing, 2016.

[17] S. Krajnović, R. Lárusson, and B. Basara. Superiority of PANS compared to LES in predicting a rudimentary landing gear flow with affordable meshes. *International Journal of Heat and Fluid Flow*, 37:109–122, 2012.

[18] G. Minelli and S. Krajnović. Numerical investigation of the actuated flow on a bluff body. In *Proceedings of the 5th International Conference on Jets, Wakes and Separated Flows (ICJWSF2015)*, pages 295–302. Springer International Publishing, 2016.

[19] M. Mirzaei, S. Krajnović, and B. Basara. Partially-averaged Navier-Stokes simulations of flows around two different Ahmed bodies. *Computers and Fluids*, 117:273 – 286, 2015.

[20] B. Basara, S. Krajnović, S. S. Girimaji, and Z. Pavlovic. Near-wall formulation of the partially averaged Navier-Stokes turbulence model. *AIAA*, 49(12):2627–2636, 2011.

[21] S. Krajnović, G. Minelli, and B. Basara. Partially-Averaged Navier-Stokes simulations of two bluff body flows. *Applied Mathematics and Computation*, 272, Part 3:692 – 706, 2016.

[22] S. Krajnović and G. Minelli. Status of PANS for bluff body aerodynamics of engineering relevance. In *Progress in Hybrid RANS-LES Modelling: Papers Contributed to the 5th Symposium on Hybrid RANS-LES Methods, 19-21 March 2014, College Station, A&M University, Texas, USA*, pages 399–410. Springer International Publishing, 2015.

[23] AVL. *FIRE CFD Solver Users Guide*. AVL GmbH, Graz, Austria, 2014.

[24] S. Krajnović and G. Minelli. Partially-Averaged Navier-Stokes simulation of the flow around simplified vehicle. In *ICNAAM 2014, 12th International Conference of Numerical Analysis and Applied Mathematics, Rhodes, Greece, Sep 22-28, 2014*, page UNSP 030019, 2015.

[25] S. Krajnović, G. Minelli, and Branislav Basara. Partially-Averaged Navier-Stokes simulation of flows around generic vehicle at yaw. In *SAE Technical Papers: SAE 2016 World Congress and Exhibition; Detroit; United States; 12 – 14 April 2016*, 2016.

[26] H. Lienhart, C. Stoots, and S. Becker. Flow and turbulence structures in the wake of a simplified car model (Ahmed model). In *DGLR Fach-Symp. AG STAB, University of Stuttgart, Germany November 1517.*, 2000.

[27] H. Lienhart, S. Becker, and C. Stoots. Flow around a simplified car body (Ahmed body) - European Research Community on Flow, Turbulance and Combustion Classsic Database. `http://cfd.mace.manchester.ac.uk/ercoftac/`, 2002. Accessed: 2017-04-01.

[28] J. Jeong and F. Hussain. On the identification of a vortex. *Journal of Fluid Mechanics*, 285:6994, 1995.

[29] Y. Kobayashi, I. Kohri, A. Kasai, T. Nasu, D. Katoh, and Y. Hashizume. Numerical analysis on the transitional mechanism of the wake structure of the Ahmed body. In *SAE Technical Paper-2016-01-1592,*. SAE International, 04 2016.